BIOCHEMISTRY
including biophysical chemistry & molecular biology

Article

pubs.acs.org/biochemistry

Subtle Dynamics of *holo* Glutamine Binding Protein Revealed with a Rigid Paramagnetic Probe

Zhu Liu,[†] Zhou Gong,[†] Da-Chuan Guo,[†] Wei-Ping Zhang,*[,‡] and Chun Tang*[,†]

[†]CAS Key Laboratory of Magnetic Resonance in Biological Systems, Wuhan Center for Magnetic Resonance, State Key Laboratory of Magnetic Resonance and Atomic Molecular Physics, Wuhan Institute of Physics and Mathematics, Chinese Academy of Sciences, Wuhan, Hubei Province 430071, China

[‡]Department of Pharmacology, Zhejiang University School of Medicine, Hangzhou, Zhejiang Province 310028, China

Supporting Information

ABSTRACT: Bacterial periplasmic binding proteins (PBPs) are involved in the translocation of small molecules in the periplasm. To unload, the two domains of a PBP open up, allowing the ligand to exit. However, it is not clear whether there are dynamics near the binding site which can facilitate the rapid dissociation of a ligand. To visualize such dynamics, we utilized paramagnetic relaxation enhancement (PRE) NMR and introduced a rigid paramagnetic probe to a PBP, glutamine-binding protein (QBP) with its cognate ligand bound. A paramagnetic Cu(II) ion is sandwiched between an engineered di-histidine motif at a helix and an NTA capping molecule. The afforded paramagnetic probe is so rigid that PRE values calculated from a single structure of *holo* QBP largely agree with the observed values. The remaining PRE discrepancies, however, manifest dynamics of a loop in the opposite domain from the paramagnetic probe. This loop packs against the glutamine ligand in the *holo* QBP and undergoes fluctuations upon ligand dissociation, as assessed by steered molecular dynamics simulations. As such, the loop dynamics, occurring for a small population in nanosecond to microsecond time scale, may be related to the ligand dissociation process. The rigid paramagnetic probe described herein can be grafted to other protein systems for structure and dynamics studies.

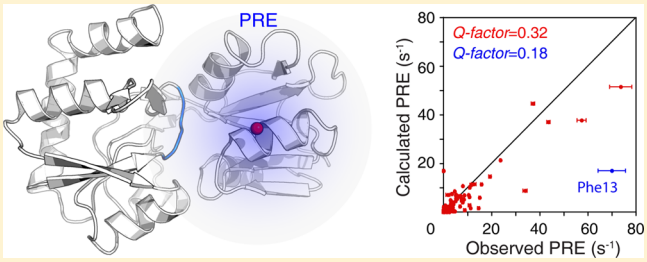

Bacterial periplasmic binding proteins (PBPs) are involved in binding and translocating different nutrients and solutes in the periplasm, such as carbohydrates, amino acids, and metal ions.[1] A PBP comprises two separately folded domains connected by a rather flexible linker. When binding to its cognate ligand, the two domains of PBP undergo hinged movement and clamp onto the ligand.[2] Maltose-binding protein (MBP) binds to maltose or maltodextrin, with a rotation of ∼35° between the two domains from the *apo* to *holo* state.[3] While at the *apo* state, MBP transiently samples a partially closed conformation,[4] which may facilitate the ligand recognition and association.[5] Another PBP, glutamine-binding protein (QBP), undergoes a ∼56° reorientation upon binding to its ligand (Figure S1, Supporting Information). However, transient domain closure for *apo* QBP was not visible to experimental inspection, possibly as a result of a more rigid linker.[6,7] In contrast, little effort has been devoted to characterize the dynamics of *holo* PBPs, regarding the mechanism for ligand dissociation and protein turnover.

A PBP binds to its ligand with a K_D value typically around 1 μM. Owing to the binding energy, a *holo* PBP is more stable than its *apo* counterpart. The binding free energy estimated for the *holo* QBP[8] amounts to −57.8 kcal/mol (Table S1, Supporting Information). For MBP, the protein is ∼16 kcal/mol more stable when adopting a *holo* closed conformation than adopting a ligand-free closed conformation.[3] Therefore, to release its ligand when docked at a membrane transporter, a *holo* PBP has to have the two domains pried open. This is triggered by a conformational switch of the associated transporter.[9] Subsequently, the ligand dissociates from PBP and is translocated through the inner membrane. However, the ligand may still be tightly bound with one of the two domains (Figure S1, Supporting Information), and it is not clear whether there are dynamics close to the binding site facilitating a seemingly passive dissociation process of the ligand.

Paramagnetic relaxation enhancement (PRE) NMR allows direct visualization of protein structure and dynamics, by attaching a paramagnetic probe at a desired site of an otherwise diamagnetic protein system.[10−12] Arising from dipolar interactions between an unpaired electron of the paramagnetic probe and protein nuclei,[13,14] PRE provides hundreds of long-range distance measurements at once. More importantly, owing to $\langle r^{-6} \rangle$ distance averaging, PRE NMR permits visualization of protein transient structure, providing a shorter distance between the probe and some part of the protein in the transient structure than in the ground-state structure.[4,15−20]

Received: November 23, 2013
Revised: February 20, 2014
Published: February 20, 2014

The observation point of PRE, a paramagnetic probe is introduced either by chemical conjugation or by protein engineering. Multiple rotatable bonds connect the paramagnetic probe and protein backbone, often resulting in a larger conformational space for the paramagnetic center. For example, the widely used MTSL probe has a distribution diameter of more than 10 Å (Figure S2, Supporting Information). The uncertainty of the paramagnetic center compromises the accuracy of the PRE distance measurement. Consequently, subtle protein dynamics with a length-scale smaller than the conformational space of the probe may not be discerned, as a compensatory movement of the probe can also account for the observed PREs. To accurately depict protein structure and to detect subtle protein dynamics, a rigid paramagnetic probe with respect to the protein is highly desirable. Hubbell and co-workers developed a series of MTSL derivatives by introducing a bulky hydrophobic group at the 4-position of the five-member ring,[21] which greatly restricts its mobility when conjugated to protein via disulfide bond.[22] Alternative, a paramagnetic probe can be introduced to protein via two attachment points, either two adjacent cysteine residues,[23,24] or one cysteine residue and an acidic residue nearby.[25,26] A paramagnetic lanthanide metal binding site has also been engineered,[27] and the probe can be rigidified with a disulfide anchor.[28]

In the present study, to visualize the dynamics of *holo* QBP, we designed a Cu(II)-based paramagnetic probe, with the metal ion sandwiched between a di-histidine motif engineered at a protein helix and a small capping molecule. The probe affords PRE measurements mostly consistent with the protein structure, which attests to the rigidity of the probe. The remaining discrepancy in PRE, however, reveals subtle dynamics of a loop in the QBP, which may be involved in ligand dissociation.

EXPERIMENTAL PROCEDURES

Protein Sample Preparation. Double histidine mutations, either 33H/37H or 140H/144H, were introduced to *E. coli* glutamine-binding protein (QBP) through site-directed mutagenesis (Stratagene). Wildtype and mutant proteins were expressed in BL21 star cells and were purified from CM fast-follow, S-100 Sephacryl, and mono-S chromatography columns in tandem (GE Healthcare). Nitrilotriacetic acid (NTA, Figure 1 inset) and other chemicals were purchased from Sinopharm. To prepare the *holo* protein, 1 mM glutamine was added throughout the purification, and unbound ligand was removed by ultrafiltration in Amicon Ultra (Millipore).

Isothermal Titration Calorimetry (ITC) Measurement. A 40 μM 140H/144H dihistidine mutant of *holo* QBP in 10 mM pH 7.5 Tris·HCl buffer containing 100 mM NaCl was placed in reservoir at 303 K on a VP-ITC (GE Healthcare) and was titrated with $CuCl_2$ at a concentration of 440 μM in the matching buffer, premixed with equimolar NTA. The first data point was removed when fitting the titration isotherms using MicroCal Origin. The dilution effect was taken into account and subtracted by titrating Cu(II)-NTA into the same buffer.

NMR Spectroscopy. Protein samples were prepared in the same buffer as ITC, and the paramagnetic sample contains 0.5 mM equimolar mixture of ^{15}N-labeled protein and Cu(II)-NTA. The data were collected on a Bruker 700 MHz or 800 MHz spectrometer equipped with a cryogenic probe at 303 K. PRE Γ_2 values for backbone amide protons were measured using a two-time-point scheme with a delay of 24 ms between the two time points.[29] The NMR spectra were processed and analyzed using NMRPipe.[30] To evaluate intermolecular contributions, PRE data were also collected for an equimolar mixture between ^{15}N-labeled wildtype and unlabeled paramagnetically tagged mutant proteins, as well as for an equimolar mixture between ^{15}N-labeled wild-type protein and Cu(II)-NTA.

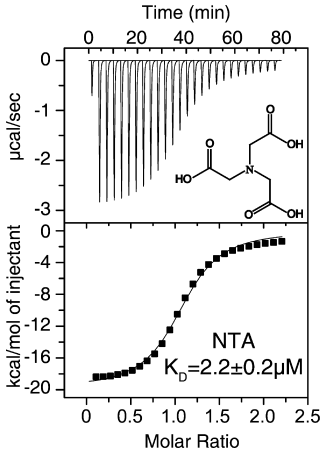

Figure 1. Dissociation constant K_D value measured using ITC, with *holo* QBP H140/H144 dihistidine mutant titrated with Cu(II) premixed with equimolar NTA. The raw data (top panel) is converted to heat per injection. The fitted curve using one-site binding model is shown as a solid line (lower panel). Inset: structure diagram of NTA.

Structure Calculation. Protein structure was taken from PDB coordinates for 1WDN,[8] and histidine mutations were introduced by editing the PDB file in PyMOL (The PyMOL Molecular Graphics System, Version 1.5 Schrödinger, LLC). The conformation for histidines and Cu(II) were optimized against bond, angle, improper, van der Waals terms, and PRE restraints using Xplor-NIH.[31] As the NTA cap is pointing out and away from the protein and only provides coordination sites for Cu(II),[32] it was not incorporated into the structural calculation. On the basis of known crystal structures of a mononuclear cupric center bound at a helix as well as a small-molecule Cu(II) ternary complex,[32] Cu(II) was restrained to be coplanar with Nε2 atoms of histidine side chains, with a Cu(II)−Nε2 bond-length of 2 Å and Nε2−Cu(II)−Nε2 angle of 90°. The starting position of Cu(II) was randomized, and the structure was refined with simulated annealing and energy minimization. Square-well energy potential was used for the PRE restraints, with no energy penalty given when the back-calculated PRE value is within ± (experimental error) of the target value. Residues with peaks broadened out beyond detection in the paramagnetic spectrum were given a large PRE value with the lower bound at 70 s^{-1}. The electron correlation τ_e for Cu(II) is ∼4.0 ns,[18,33] and the isotropic rotational correlation time of *holo* QBP τ_r is measured at ∼12 ns, affording an estimated PRE correlation time of 3.0 ns.[13,14] PRE Q-factor assesses the differences between observed and calculated PRE values,[10,29] with the experimental errors also taken into account, that is, no contribution to the increase of PRE Q-factor if the back-calculated value is within ± (experimental error) of the target value. Structures were illustrated in PyMOL.

Steered MD Simulation. Binding energy analysis using MMPBSA scheme was performed in AMBER 12 package. The domain 1 structure (comprising residues 1−88 and 183−226) was generated from the structure of *holo* QBP[8] with the ligand

dx.doi.org/10.1021/bi4015715 | *Biochemistry* 2014, 53, 1403−1409

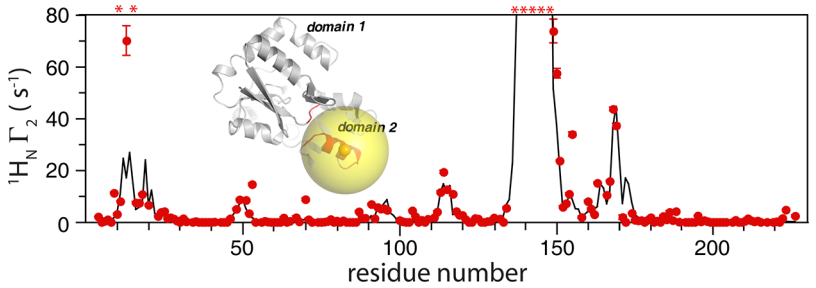

Figure 2. PRE Γ_2 values measured for backbone amide protons of *holo* QBP, with the Cu(II) paramagnetic probe introduced at the 140H/144H site. The red spheres denote observed values; the back line denotes calculated PRE values from protein structure; asterisks denote residues completely broadened out in the paramagnetic spectrum. Inset: isosurface with Γ_2 = 50 s^{-1} centered at Cu(II) is indicated by a 12 Å radius yellow sphere on the *holo* QBP structure; residues with measured PRE Γ_2 value > 50 s^{-1} are in red.

still bound, after removing the residues for domain 2 (comprising residues 89−182). The β-hairpin structure at the linker was stitched together with a Gly-Thr dipeptide, to generate a continuous polypeptide strand (Figure S3, Supporting Information). Conventional MD (cMD) and steered MD (sMD) were carried out in the AMBER 12 with ff12SB force field. The protein was first solvated in a cube box containing the TIP3P water molecules, with an 8 Å padding in all directions. The time step was set at 2 fs, and the SHAKE algorithm was used to constrain the bonds connecting hydrogen atoms. The Langevin thermostat was used to control the temperature using a collision frequency of 1.0/ps for cMD and 5.0/ps for sMD.[34] The long-range electrostatics was treated with the particle mesh Ewald (PME) method[35] with default Ewald parameters and with a van der Waals cutoff of 10 Å. The final structure from 2 ns cMD simulation was used as the input structure for 200 ns more of either cMD or sMD simulations. The sMD simulations were performed using a scheme similar to umbrella sampling, with the time-dependent restraint as defined in this equation $V(t) = 1/2k[x - x_0(t)]^2$, in which x is the distance between the Cα of glutamine ligand and the Cα of residue A12 or Y86, and k is given at 5 kcal·mol^{-1}·$Å^{-1}$ for a soft elastic spring.

RESULTS

Attachment of a Cu(II) Paramagnetic Probe. We engineered a double-histidine mutation to the periplasmic binding protein QBP of *Escherichia coli*. Both histidine mutations are located at one side of a helix and are solvent exposed. With an NTA cap, we assessed the stability of the resulted protein-metal complexes using isothermal calorimetry (ITC) titration. The stability constant between Cu(II) chelate and NTA is femtomolar,[36,37] orders of magnitude stronger than the interaction between Cu(II) and protein. As such, with Cu(II) and NTA premixed at 1:1 ratio, the binding between the di-histidine mutant of *holo* QBP and Cu(II)-NTA can be treated as a bimolecular event, affording a K_D value of 2.2 ± 0.2 μM (Figure 1). The NTA cap completes the metal coordination sites. Indeed, in the absence of a cap, the ITC binding isotherm can be fitted to a 1:2 stoichiometry between Cu(II) and protein, with the titration midpoint at 0.5 stoichiometry and an apparent K_D value of 3.4 ± 0.3 μM for each binding site (Figure S4, Supporting Information). It is likely that such 1:2 complex is formed with Cu(II) sandwiched between two di-histidine mutant proteins.[37,38]

Cu(II) PREs Mostly Agree with Protein Structure. We then measured the transverse PRE Γ_2 rates for amide protons of *holo* QBP (Figure 2), with the probe introduced at H140/H144 site. Large PRE values were observed for residues near the probe, with residues 138−149 completely broadened out beyond detection. In general, PREs were observed for residues within ~20 Å radius of the Cu(II) ion, and residues with PRE Γ_2 > 50 s^{-1} are located within a 12 Å radius of the paramagnetic center (Figure 2 inset). Surprisingly, loop residues 12−14, which are located in the opposite domain and are far from the probe, also experience large PREs.

To account for the observed Cu(II) PREs, we modeled the structure for the ternary complex comprising NTA, Cu(II), and QBP mutant. On the basis of known PDB structures containing a mononuclear cupric center at a protein helix,[38−45] Cu(II) was restrained to be coplanar with each histidine imidazole ring, with additional bond length, bond angle, and improper terms applied. Starting from the crystal structure for *holo* QBP[8] and by refining against covalent and nonbonded energy terms, a single defined structure for the paramagnetic probe is obtained, which is sufficient to account for most observed PREs (Figure 2, solid line), with a PRE Q-factor of 0.32 (Figure 3A). No matter what the starting coordinates of Cu(II) are in respect to the protein, the calculation converged to a same structure. In this structure (Figure 3B), the (χ_1, χ_2) dihedral angles for residues H140 and H144 are (−175.3°, 78.7°) and (−94.6°, −52.6°), respectively. Invoking more than one conformer to represent the probe,[10,29] however, does not lead to an

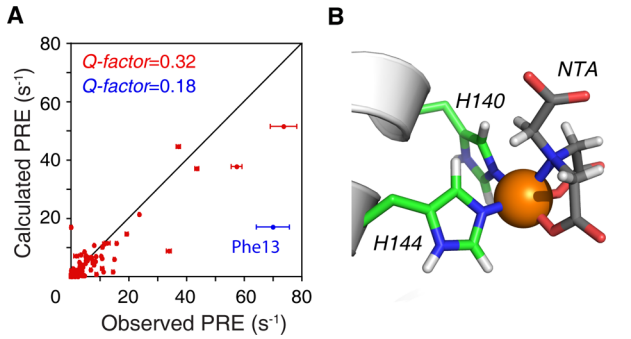

Figure 3. Observed PREs for *holo* QBP can be mostly accounted for with a single-conformer representation for the Cu(II) paramagnetic probe. (A) Correlation between observed and calculated ^1H Γ_2 values. The PRE Q-factor can be improved to 0.18 by excluding loop residues 12−14. (B) The optimized structure for the ternary Cu(II) complex with an NTA cap. Protein helix is shown as cartoon, histidine side chains and NTA shown as sticks, and Cu(II) shown as an orange sphere.

dx.doi.org/10.1021/bi4015715 | *Biochemistry* 2014, 53, 1403−1409

improvement of PRE Q-factor, with the positions of Cu(II) clustering at identical positions.

We then introduced the Cu(II) paramagnetic probe at a second site, H33/H37 site in domain 1, and measured PRE Γ_2 rates of amine protons for this di-histidine mutant (Figure S5A, Supporting Information). After optimizing covalent geometry and noncovalent terms, the (χ_1, χ_2) dihedral angles for residues H33 and H37 converge to (−169.0°, 73.0°) and (−99.7°, −47.6°), respectively (Figure S5B, Supporting Information). On the basis of this structure, the calculated PRE values largely agree with observed values. With both observed and calculated PRE Γ_2 values less than 5 s^{-1}, we do not see PRE discrepancies for loop residues 12−14 (Figure S5C, Supporting Information).

PRE Discrepancy for a Loop Domain 1 Manifests Protein Dynamics. Though largely agreeing with the *holo* QBP crystal structure, the agreement between observed and calculated PREs can be improved to a Q-factor of 0.18, simply by excluding residues A12, F13, and V14 in the calculation (Figure 3A). Structural refinement without PRE restraints for these residues afforded an almost identical position for the Cu(II) ion and the same PRE Q-factor, as the refinement against all the PRE restraints. Residues 12−14 are located in a loop in the domain 1 of QBP, about 13 Å away from the paramagnetic center (Figure 2 inset). The large PRE values observed for these residues did not result from nonspecific interactions between the protein and the probe, as the addition of equimolar Cu(II)-NTA mixture to wildtype QBP does not cause PREs to these residues (Figure S6, Supporting Information). On the other hand, no intermolecular PREs were observed for ^{15}N-labeled wildtype *holo* QBP mixed with equimolar unlabeled, paramagnetically tagged mutant protein (Figure S7, Supporting Information).

To determine the cause for the PRE discrepancies, we measured residual dipolar couplings (RDCs) for the wildtype *holo* QBP. The observed RDC values agree well with the calculated values from the crystal structure,[8] affording an *R*-factor of 20.99 and correlation coefficient of 0.961. The level of agreement is expected for a crystal structure at this resolution (1.94 Å).[46,47] In particular, the RDC values for the residues 12−14 agree well between observed and calculated values (Figure S8, Supporting Information).

The loop residues appear rigid on the picosecond−nanosecond time scale, as shown by backbone ^{15}N heteronuclear NOE measurement (Figure S9, Supporting Information). In addition, conventional MD simulations up to 200 ns failed to reveal any significant motion for these residues (Figure S10, Supporting Information). On the other hand, CPMG relaxation dispersion experiment[48] failed to reveal any exchange contributions to the effective transverse ^{15}N relaxation rates in the millisecond time scale (Figure S11, Supporting Information). Taken together, the PRE discrepancies for the *holo* QBP should arise from a small population of alternative protein conformation in exchange with protein ground-state structure at the nanosecond−microsecond time scale.

To understand the functional relevance of the dynamics involving the loop residues in the domain 1, we conducted steered MD (sMD) simulations for the *holo* QBP. By applying a weak constraint on the ligand in a direction away from the protein, sMD recapitulates protein dynamics during glutamine dissociation at a time scale that is otherwise too long for conventional MD simulation (Figure S10, Supporting Information). When the two domains of a PBP are pried open,[9] the ligand likely remains associated with one of the two domains. It has been shown that the maltose preferably binds to the C-terminal domain of *holo* MBP when the protein is crystallized in an open conformation.[49] Likewise for QBP, the domain 1 contributes twice as much binding energy toward glutamine as the domain 2 (Table S1, Supporting Information) and likely retains the ligand when the two domains are pried open. Therefore, we removed the domain 2 from the *holo* QBP structure to better visualize the dissociation process and to create an exit route for the ligand. The remaining residues of domain 1 (1−88 and 183−226) are stitched back with a Gly-Thr dipeptide, thus to generate a continuous linear polypeptide (Figure S3, Supporting Information). No matter which steering direction is applied, a similar pattern for protein dynamics can be observed (Figure 4). Residues 12−14 display the largest

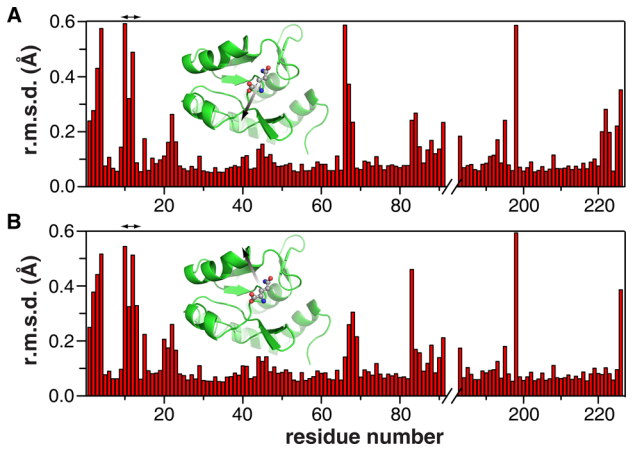

Figure 4. Steered MD simulations recapitulating ligand dissociation process from the domain 1 of *holo* QBP. The gray arrow indicates the direction of steering, either A, along the Cα of A12 to Cα of the glutamine ligand, or B, along the Cα of Y86 to Cα of the glutamine ligand. The r.m.s. deviations for backbone heavy atoms were calculated from 2000 evenly spaced snapshots in a 200 ns simulation. The loop residues in the domain 1 are indicated.

fluctuations of backbone heavy atoms, close to 0.6 Å on average, during the ligand dissociation process—the displacement for the backbone amide proton of F13 can be as large as 1.8 Å with the phenyl ring completely swinging out (Figure S12, Supporting Information). Loop residues A12 and V14 as well as D10 and T11 can have a ∼2 Å displacement for their amide protons during the sMD simulation. Outside the loop, some residues also display large backbone r.m.s. deviations during the simulation, including the N-terminal residues. Yet these residues are already dynamic at the picosecond−nanosecond time scale, as assessed from the ^{1}H−^{15}N heteronuclear NOE (Figure S8, Supporting Information).

DISCUSSION

Using a rigid paramagnetic probe, we observed dynamic fluctuation for a loop in the domain 1 of *holo* QBP, which gave rise to the discrepancy between observed and calculated PRE values. Owing to $\langle r^{-6} \rangle$ distance dependence of PRE, a small decrease in the probe−nuclei distance can result in a large increase in the PREs.[10] Thus, to account for the PRE discrepancies, a small population of the loop residues, including A12, F13, and V14, should transiently move toward the probe in the domain 2 (Figure 5). The dynamics are quite subtle, probably on the length-scale of a few angstroms, which have

dx.doi.org/10.1021/bi4015715 | *Biochemistry* 2014, 53, 1403−1409

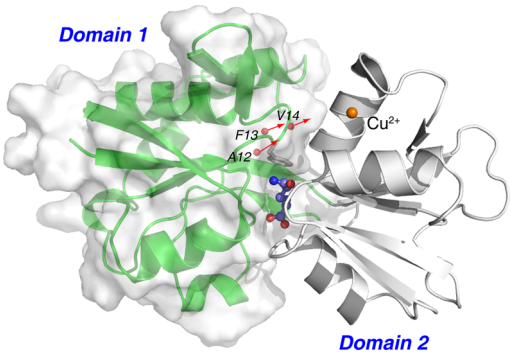

Figure 5. Loop motion in the QBP domain 1 may be involved in the ligand dissociation process. Protein structure is shown as cartoon, and the glutamine ligand is shown as balls-and-sticks. The Cu(II) paramagnetic center and amide protons of the loop residues are shown as spheres. The phenyl ring of F13, shown as gray sticks, packs against the amide group of the glutamine ligand. Red arrows indicate the possible direction of movement of the loop residues.

eluded the previous studies using a MTSL probe.[6,7] The MTSL probe takes up a large conformational space (Figure S2, Supporting Information), and a compensatory movement of the probe would also account for the subtle fluctuation of protein structure, affording a reasonably good PRE Q-factor. On the basis of MD simulations, heteronuclear NOE, and relaxation dispersion measurements, the dynamic fluctuation of the loop residues likely occurs at the nanosecond-microsecond time scale or supra-τ_c time scale. With the Cu(II) probe attached at a second site, 33H/37H in the domain 1 of *holo* QBP, the PRE values observed for the loop residues largely agree with the calculated values (Figure S5A, Supporting Information). This is because the PRE values for these residues are already quite small, and the loop is possibly moving away from the probe in the domain 1 and toward the domain 2.

The dynamics of this loop may be coupled with ligand dissociation from *holo* QBP. In the crystal structure,[8] the phenyl ring of F13 packs against a bound glutamine (Figure 5). Therefore, subtle movement of the loop may help to dislodge the ligand, or alternatively, dissociation of the ligand may perturb the conformation of the loop. Indeed, our sMD simulations showed that these residues in the domain 1 experience large amplitude of fluctuations as glutamine leaves the binding pocket. As such, detachment of the ligand from the tightly bound domain of QBP may be facilitated by the dynamics of these loop residues. Indeed, in many other protein systems, it has been shown that loop dynamics modulate ligand exit,[50] enzyme activity,[51] and channel gating.[52]

Elucidation of the subtle dynamics in *holo* QBP was made possible with a rigidly attached Cu(II)-based paramagnetic probe. Cupric metal centers are found in many proteins as structural and catalytic cofactors.[40−44] For a mononuclear cupric center at a protein helix, Cu(II) is coordinated to Nε2 atoms of two histidines separated by three residues.[32,38−45] Inspired, Cu(II)-binding motif has been engineered to protein helix through site-directed mutagenesis[38,45] On the other hand, Cu(II) can also mediate juxtaposition of two helices.[38] Therefore, an NTA capping molecule is essential to complete the metal coordination and to prevent protein dimerization.

Compared to thiol-linked probes, our Cu(II)-based probe has fewer rotatable bonds and preferred side chain rotamers and can be further stabilized with the coordination of the capping molecule. As a result, we have shown that a single structure of the paramagnetic probe accounts for most observed PREs. In contrast, multiple-conformer representation is needed to represent the large conformational space of MTSL and other paramagnetic probes.[10] When introduced to a second helical site in QBP, our Cu(II)-based probe adopts an essentially identical structure, with (χ_1, χ_2) dihedral angles differing by only ~5° from the structure at the first site. Thus, this probe can be readily grafted to other protein systems, for structure and dynamics characterization.

Taken together, the loop dynamics revealed by the rigid paramagnetic probe may be coupled to ligand dissociation from the *holo* QBP. Elucidation of subtle protein dynamics would afford a better understanding of the mechanism for protein function.

■ ASSOCIATED CONTENT

Supporting Information

A table showing MMPBSA analysis for *holo* QBP, a figure showing the rigid-body rotation of QBP, a figure showing the spread of MTSL, a figure showing the definition of domain 1 and 2 in QBP, an ITC titration curve obtained in the absence of NTA, PRE data with the probe attached at a second site, two control plots showing the absence of intermolecular PREs, RDC analysis plot for the protein, a plot showing ^{15}N heteronuclear NOEs, conventional MD simulation analysis plot, a figure showing the displacement of domain 1 loop in the sMD simulation. This material is available free of charge via the Internet at http://pubs.acs.org.

■ AUTHOR INFORMATION

Corresponding Authors

*(C.T.) tanglab@wipm.ac.cn. Phone: 86-27-87197133.
*(W.-P.Z.) weiping601@zju.edu.cn.

Funding

The work was supported by the Ministry of Science and Technology of China (2013CB910200 and 2009CB918600), the National Natural Sciences Foundation of China (31225007, 21073230 and 31170728), and the Chinese Academy of Sciences (KJCX2-EW-W05). C.T. is a Howard Hughes Medical Institute (HHMI) International Early Career Scientist.

Notes

The authors declare no competing financial interest.

■ ABBREVIATIONS

PBP, periplasmic binding proteins; QBP, glutamine-binding protein; NMR, nuclear magnetic resonance; RDC, residual dipolar coupling; PRE, paramagnetic resonance enhancement; MD, molecular dynamics; MMPBSA, molecular mechanic Poisson−Boltzmann surface area; ITC, isothermal calorimetry; NTA, nitrilotriacetic acid

■ REFERENCES

(1) Tam, R., and Saier, M. H., Jr. (1993) Structural, functional, and evolutionary relationships among extracellular solute-binding receptors of bacteria. *Microbiol. Rev. 57*, 320−346.

(2) Dwyer, M. A., and Hellinga, H. W. (2004) Periplasmic binding proteins: a versatile superfamily for protein engineering. *Curr. Opin. Struct. Biol. 14*, 495−504.

(3) Millet, O., Hudson, R. P., and Kay, L. E. (2003) The energetic cost of domain reorientation in maltose-binding protein as studied by NMR and fluorescence spectroscopy. *Proc. Natl. Acad. Sci. U. S. A. 100*, 12700−12705.

(4) Tang, C., Schwieters, C. D., and Clore, G. M. (2007) Open-to-closed transition in apo maltose-binding protein observed by paramagnetic NMR. *Nature 449*, 1078−1082.
(5) Bucher, D., Grant, B. J., and McCammon, J. A. (2011) Induced fit or conformational selection? The role of the semi-closed state in the maltose binding protein. *Biochemistry 50*, 10530−10539.
(6) Bermejo, G. A., Strub, M. P., Ho, C., and Tjandra, N. (2009) Determination of the solution-bound conformation of an amino acid binding protein by NMR paramagnetic relaxation enhancement: use of a single flexible paramagnetic probe with improved estimation of its sampling space. *J. Am. Chem. Soc. 131*, 9532−9537.
(7) Bermejo, G. A., Strub, M. P., Ho, C., and Tjandra, N. (2010) Ligand-free open-closed transitions of periplasmic binding proteins: the case of glutamine-binding protein. *Biochemistry 49*, 1893−1902.
(8) Sun, Y. J., Rose, J., Wang, B. C., and Hsiao, C. D. (1998) The structure of glutamine-binding protein complexed with glutamine at 1.94 A resolution: comparisons with other amino acid binding proteins. *J. Mol. Biol. 278*, 219−229.
(9) Oldham, M. L., and Chen, J. (2011) Crystal structure of the maltose transporter in a pretranslocation intermediate state. *Science 332*, 1202−1205.
(10) Clore, G. M., and Iwahara, J. (2009) Theory, Practice, and Applications of Paramagnetic Relaxation Enhancement for the Characterization of Transient Low-Population States of Biological Macromolecules and Their Complexes. *Chem. Rev. 109*, 4108−4139.
(11) Otting, G. (2010) Protein NMR using paramagnetic ions. *Annu. Rev Biophys. 39*, 387−405.
(12) Keizers, P. M., and Ubbink, M. (2011) Paramagnetic tagging for protein structure and dynamics analysis. *Prog. Nucl. Magn. Reson. Spectrosc. 58*, 88−96.
(13) Solomon, I. (1955) Relaxation processes in a system of two spins. *Phys. Rev. 99*, 559−565.
(14) Bloembergen, N. (1957) Proton relaxation times in paramagnetic solutions. *J. Chem. Phys. 27*, 572−573.
(15) Iwahara, J., and Clore, G. M. (2006) Detecting transient intermediates in macromolecular binding by paramagnetic NMR. *Nature 440*, 1227−1230.
(16) Tang, C., Iwahara, J., and Clore, G. M. (2006) Visualization of transient encounter complexes in protein-protein association. *Nature 444*, 383−386.
(17) Tang, C., Louis, J. M., Aniana, A., Suh, J. Y., and Clore, G. M. (2008) Visualizing transient events in amino-terminal autoprocessing of HIV-1 protease. *Nature 455*, 693−696.
(18) Yu, D. M., Volkov, A. N., and Tang, C. (2009) Characterizing dynamic protein-protein interactions using differentially scaled paramagnetic relaxation enhancement. *J. Am. Chem. Soc. 131*, 17291−17297.
(19) Baldwin, A. J., and Kay, L. E. (2009) NMR spectroscopy brings invisible protein states into focus. *Nat. Chem. Biol. 5*, 808−814.
(20) Liu, Z., Zhang, W. P., Xing, Q., Ren, X., Liu, M., and Tang, C. (2012) Noncovalent dimerization of ubiquitin. *Angew. Chem., Int. Ed. Engl. 51*, 469−472.
(21) Columbus, L., Kalai, T., Jeko, J., Hideg, K., and Hubbell, W. L. (2001) Molecular motion of spin labeled side chains in alpha-helices: analysis by variation of side chain structure. *Biochemistry 40*, 3828−3846.
(22) Fawzi, N. L., Fleissner, M. R., Anthis, N. J., Kalai, T., Hideg, K., Hubbell, W. L., and Clore, G. M. (2011) A rigid disulfide-linked nitroxide side chain simplifies the quantitative analysis of PRE data. *J. Biomol. NMR 51*, 105−114.
(23) Keizers, P. H., Saragliadis, A., Hiruma, Y., Overhand, M., and Ubbink, M. (2008) Design, synthesis, and evaluation of a lanthanide chelating protein probe: CLaNP-5 yields predictable paramagnetic effects independent of environment. *J. Am. Chem. Soc. 130*, 14802−14812.
(24) Swarbrick, J. D., Ung, P., Su, X. C., Maleckis, A., Chhabra, S., Huber, T., Otting, G., and Graham, B. (2011) Engineering of a bis-chelator motif into a protein alpha-helix for rigid lanthanide binding and paramagnetic NMR spectroscopy. *Chem. Commun. 47*, 7368−7370.
(25) Su, X. C., Man, B., Beeren, S., Liang, H., Simonsen, S., Schmitz, C., Huber, T., Messerle, B. A., and Otting, G. (2008) A dipicolinic acid tag for rigid lanthanide tagging of proteins and paramagnetic NMR spectroscopy. *J. Am. Chem. Soc. 130*, 10486−10487.
(26) Swarbrick, J. D., Ung, P., Chhabra, S., and Graham, B. (2011) An iminodiacetic acid based lanthanide binding tag for paramagnetic exchange NMR spectroscopy. *Angew. Chem., Int. Ed. Engl. 50*, 4403−4406.
(27) Nitz, M., Sherawat, M., Franz, K. J., Peisach, E., Allen, K. N., and Imperiali, B. (2004) Structural origin of the high affinity of a chemically evolved lanthanide-binding peptide. *Angew. Chem., Int. Ed. Engl. 43*, 3682−3685.
(28) Saio, T., Ogura, K., Yokochi, M., Kobashigawa, Y., and Inagaki, F. (2009) Two-point anchoring of a lanthanide-binding peptide to a target protein enhances the paramagnetic anisotropic effect. *J. Biomol. NMR 44*, 157−166.
(29) Iwahara, J., Tang, C., and Clore, G. M. (2007) Practical aspects of 1H transverse paramagnetic relaxation enhancement measurements on macromolecules. *J. Magn. Reson. 184*, 185−195.
(30) Delaglio, F., Grzesiek, S., Vuister, G. W., Zhu, G., Pfeifer, J., and Bax, A. (1995) NMRPipe: a multidimensional spectral processing system based on UNIX pipes. *J. Biomol. NMR 6*, 277−293.
(31) Schwieters, C. D., Kuszewski, J. J., Tjandra, N., and Clore, G. M. (2003) The Xplor-NIH NMR molecular structure determination package. *J. Magn. Reson. 160*, 65−73.
(32) Burns, C. J., Field, L. D., Hambley, T. W., Lin, T., Ridley, D. D., Turner, P., and Wilkinson, M. P. (2001) X-Ray crystal structural determination of copper(II)-nitrilotriacetic acid-bis(N-methylimidazol-2-yl)ketone ternary complex. *ARKIVOC vii*, 157−165.
(33) Donaldson, L. W., Skrynnikov, N. R., Choy, W. Y., Muhandiram, D. R., Sarkar, B., Forman-Kay, J. D., and Kay, L. E. (2001) Structural characterization of proteins with an attached ATCUN motif by paramagnetic relaxation enhancement NMR spectroscopy. *J. Am. Chem. Soc. 123*, 9843−9847.
(34) Loncharich, R. J., Brooks, B. R., and Pastor, R. W. (1992) Langevin dynamics of peptides: the frictional dependence of isomerization rates of N-acetylalanyl-N'-methylamide. *Biopolymers 32*, 523−535.
(35) Essmann, U., Perera, L., Berkowitz, M. L., Darden, T., Lee, H., and Pedersen, L. G. (1995) A Smooth Particle Mesh Ewald Method. *J. Chem. Phys. 103*, 8577−8593.
(36) Anderegg, G. (1982) Critical Survey of Stability-Constants of NTA Complexes. *Pure Appl. Chem. 54*, 2693−2758.
(37) Anderegg, G., Arnaud-Neu, F., Delgado, R., Felcman, J., and Popov, K. (2005) Critical evaluation of stability constants of metal complexes of complexones for biomedical and environmental applications. *Pure Appl. Chem. 77*, 1445−1495.
(38) Salgado, E. N., Ambroggio, X. I., Brodin, J. D., Lewis, R. A., Kuhlman, B., and Tezcan, F. A. (2010) Metal templated design of protein interfaces. *Proc. Natl. Acad. Sci. U. S. A. 107*, 1827−1832.
(39) Arnold, F. H., and Haymore, B. L. (1991) Engineered metal-binding proteins: purification to protein folding. *Science 252*, 1796−1797.
(40) Hazes, B., Magnus, K. A., Bonaventura, C., Bonaventura, J., Dauter, Z., Kalk, K. H., and Hol, W. G. (1993) Crystal structure of deoxygenated Limulus polyphemus subunit II hemocyanin at 2.18 Å resolution: clues for a mechanism for allosteric regulation. *Protein Sci. 2*, 597−619.
(41) Gomis-Ruth, F. X., Grams, F., Yiallouros, I., Nar, H., Kusthardt, U., Zwilling, R., Bode, W., and Stocker, W. (1994) Crystal structures, spectroscopic features, and catalytic properties of cobalt(II), copper(II), nickel(II), and mercury(II) derivatives of the zinc endopeptidase astacin. A correlation of structure and proteolytic activity. *J. Biol. Chem. 269*, 17111−17117.
(42) Cuff, M. E., Miller, K. I., van Holde, K. E., and Hendrickson, W. A. (1998) Crystal structure of a functional unit from Octopus hemocyanin. *J. Mol. Biol. 278*, 855−870.

(43) Moroz, O. V., Antson, A. A., Grist, S. J., Maitland, N. J., Dodson, G. G., Wilson, K. S., Lukanidin, E., and Bronstein, I. B. (2003) Structure of the human S100A12-copper complex: implications for host-parasite defence. *Acta Crystallogr., Sect. D: Biol. Crystallogr. 59*, 859−867.
(44) Matoba, Y., Bando, N., Oda, K., Noda, M., Higashikawa, F., Kumagai, T., and Sugiyama, M. (2011) A molecular mechanism for copper transportation to tyrosinase that is assisted by a metal-lochaperone, caddie protein. *J. Biol. Chem. 286*, 30219−30231.
(45) Huard, D. J., Kane, K. M., and Tezcan, F. A. (2013) Re-engineering protein interfaces yields copper-inducible ferritin cage assembly. *Nat. Chem. Biol. 9*, 169−176.
(46) Bax, A. (2003) Weak alignment offers new NMR opportunities to study protein structure and dynamics. *Protein Sci. 12*, 1−16.
(47) Simon, K., Xu, J., Kim, C., and Skrynnikov, N. R. (2005) Estimating the accuracy of protein structures using residual dipolar couplings. *J. Biomol. NMR 33*, 83−93.
(48) Mittermaier, A., and Kay, L. E. (2006) New tools provide new insights in NMR studies of protein dynamics. *Science 312*, 224−228.
(49) Duan, X., and Quiocho, F. A. (2002) Structural evidence for a dominant role of nonpolar interactions in the binding of a transport/chemosensory receptor to its highly polar ligands. *Biochemistry 41*, 706−712.
(50) Wang, T., and Duan, Y. (2009) Ligand entry and exit pathways in the beta2-adrenergic receptor. *J. Mol. Biol. 392*, 1102−1115.
(51) Kunze, M. B., Wright, D. W., Werbeck, N. D., Kirkpatrick, J., Coveney, P. V., and Hansen, D. F. (2013) Loop interactions and dynamics tune the enzymatic activity of the human histone deacetylase 8. *J. Am. Chem. Soc. 135*, 17862−17868.
(52) Zhuang, T., Chisholm, C., Chen, M., and Tamm, L. K. (2013) NMR-based conformational ensembles explain pH-gated opening and closing of OmpG channel. *J. Am. Chem. Soc. 135*, 15101−15113.